ADDITIVE MANUFACTURING OF BI-CONTINUOUS PIEZOCOMPOSITES WITH TRIPLY PERIODIC PHASE INTERFACES FOR COMBINED FLEXIBILITY AND PIEZOELECTRICITY

Xuan Song[1,*], Li He[1], Wenhua Yang[2], Zhuo Wang[2], Zeyu Chen[3], Jing Guo[4,5], Hong Wang[6], Lei Chen[2,*]

[1]Department of Industrial and Systems Engineering, Center for Computer Aided Design, University of Iowa, Iowa City, IA, USA

[2]Department of Mechanical Engineering, Mississippi State University, Mississippi State, MS, USA

[3]Department of Biomedical Engineering, University of Southern California, Los Angeles, CA, USA

[4]Materials Research Institute, the Pennsylvania State University, University Park, PA, USA

[5]School of Materials Science and Engineering, Xi'an Jiaotong University, Xi'an, China

[6]Materials Science and Technology Division, Oak Ridge National Laboratory, Oak Ridge, TN, USA
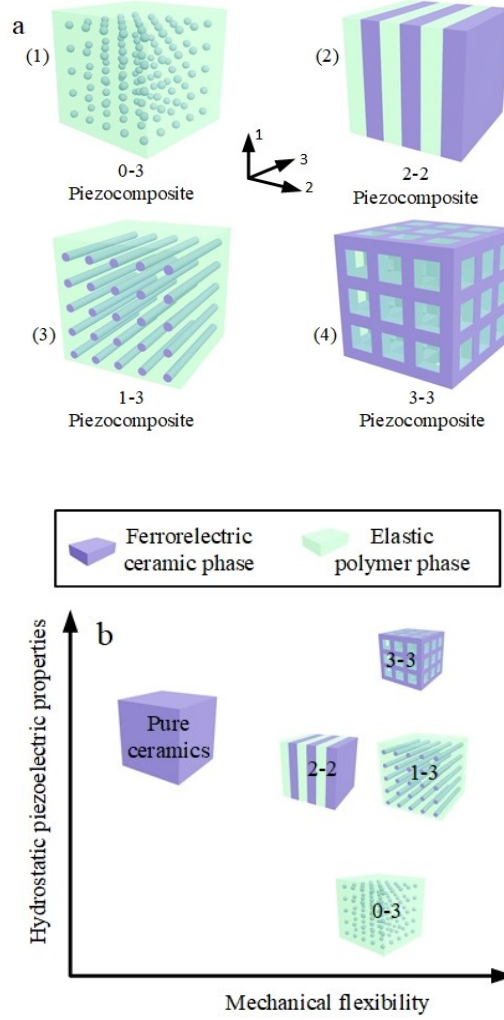
Abstract:

An additive manufacturing-enabled bi-continuous piezocomposite architecture is presented to achieve mechanical flexibility and piezoelectricity simultaneously in piezoelectric materials. This architecture is comprised of an active ferroelectric ceramic phase and a passive flexible polymer phase, which are separated by a tailorable phase interface. Triply periodic minimal surfaces were used to define the phase interface, due to their excellent elastic properties and load transfer efficiency. A suspension-enclosing projection-stereolithography process was used to additively manufacture this material. Post processes including polymer infiltration, electroding and poling are introduced. Piezoelectric properties of the piezocomposites are numerically and experimentally studied. The results highlight the role of tailorable triply periodic phase interfaces in promoting mechanical flexibility and piezoelectricity of bi-continuous piezocomposites.

1. Introduction

Mechanical flexibility and piezoelectricity are two seemingly conflicting properties existing in state-of-the-art piezoelectric materials that produce electrical signals in response to applied mechanical stress. For example, ferroelectric ceramics, such as Lead Zirconate Titanate (PZT) and Barium Titanate (BTO), possess excellent piezoelectric properties, but are extremely brittle in response to mechanical shocks or tensile strains [1-4]; piezoelectric polymers, such as polyvinylidene difluoride (PVDF), are sufficiently flexible to withstand mechanical shocks but typically have poor energy conversion efficiency [5, 6]. This conflict limits the application of piezoelectric devices under harsh environments and extreme loading conditions. There is a need for next generation piezoelectric materials exhibiting a good property combination of mechanical flexibility and piezoelectricity.

A typical strategy to achieve a piezoelectric material with both mechanical flexibility and piezoelectricity is to combine ferroelectric ceramics with elastic polymers and form a *piezocomposite*. The elastic polymer phase increases flexibility of the materials [7], while the ceramic phase introduces large piezoelectric properties to the composite. Based on the connectivity patterns between the ceramic and polymer phases [8, 9], piezocomposites can be represented by an index of two numbers, e.g. 1-3, as shown in Figure 1a. The first number indicates the dimension in which the active phase (i.e. ferroelectric ceramic) is self-connected and the second number denotes the dimension in which the passive phase (i.e. elastic polymer) is self-connected. Of all the most studied connectivity patterns, including 0-3 [10-12], 1-3 [13], 2-2 [14] and 3-3 [15-17], 3-3 piezocomposites appear to be a promising architecture which have demonstrated higher piezoelectric performance than the others. Of particular interest is their superb hydrostatic piezoelectric properties as depicted in Figure 1b, which may find uses in applications of underwater acoustic devices (i.e. hydrophone).

A 3-3 piezocomposite has its two phases interconnected in three-dimension (3D) and is hence called *bi-continuous piezocomposite*. In such a material, the interface between the two phases is a 3D continuous surface. According to our recent work [18], the geometry of the phase interface of a bi-continuous piezocomposite plays an important role in promoting its piezoelectric properties. However, traditional bi-continuous piezocomposites are usually produced by manufacturing a porous piezoelectric-ceramic structure via conventional foam fabrication techniques and subsequently impregnating the porosity with a polymer [17, 19-21]. The resultant structures possess a poor 3D interconnectivity between the phases and thereby attain an unconnected phase interface [17, 19-21]. With such a phase interface, the potential of bi-continuous architectures in enhancing mechanical flexibility and piezoelectricity has not yet been fully exploited to date.

Figure 1. Constructions and properties of piezoelectric composites. (1) Main connectivity patterns of piezoelectric composites; (2) comparisons of piezoelectric materials in hydrostatic piezoelectric properties and mechanical flexibility.

The aim of this paper is to present an alternative bi-continuous piezocomposite with a fully 3D continuous phase interface defined by triply periodic minimal surfaces. These interfaces provide significantly higher stress transfer efficiency with respect to the traditional porous interfaces, which subsequently contributes to the superior piezoelectric properties (in particular hydrostatic piezoelectricity) of the piezocomposite. Moreover, a new additive manufacturing (AM) is utilized to achieve a phase interface of any desired geometry in a piezocomposite. The paper is organized as follows: design of the new 3-3 piezocomposite structures is introduced in section 2; fabrication of the 3-3 piezocomposites is presented in section 3; numerical and experimental analysis of the structures are introduced in section 4; analytical results are given in section 5; conclusions and future work are discussed in section 6.

2. Design method

A bi-continuous piezocomposite is composed of a ferroelectric ceramic phase and a flexible polymer phase. The ferroelectric ceramic phase contributes to the final piezoelectricity of the piezocomposite material, and the polymer phase determines the mechanical flexibility. The overall physical properties of the piezocomposite are dependent on the morphologies of the interfaces between the two phases.

In recent years, there has been a growing interest in designing the interfaces of bi-continuous composites with triply periodic minimal surfaces [22-24] for enhanced mechanical properties. These surfaces provide better elastic properties and load transfer and exhibit a unique combination of stiffness, strength and energy absorption as compared to the other geometric arrangements of the constituents[23]. These excellent properties offer the potential to produce flexible piezocomposites with high piezoelectricity. Inspired by these studies, we employ triply periodic minimal surfaces to design the phase interfaces of bi-continuous piezocomposites. The achieved bi-continuous piezocomposites are named as triply periodic bi-continuous (TPC) piezocomposite.

According to the previous studies [22, 25, 26], triply periodic minimal surfaces can be approximated by the well-established level set structures. In this paper, three types of level set structures are considered, including simple cubic (SC), face-centered-cubic (FCC) and body-centered-cubic (BCC), as shown in Figure 2. These three level set structures are defined by the following equations:
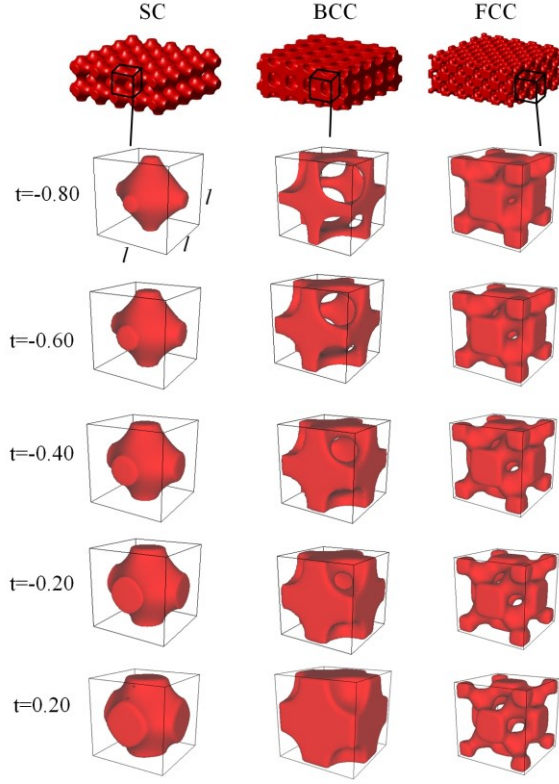
$$f_{sc}(x,y,z) = \cos\left(\frac{2\pi x}{l}\right) + \cos\left(\frac{2\pi y}{l}\right) + \cos\left(\frac{2\pi z}{l}\right) + t = 0 \tag{1}$$

$$f_{bcc}(x,y,z) = \cos\left(\frac{2\pi x}{l}\right)\cos\left(\frac{2\pi y}{l}\right) + \cos\left(\frac{2\pi y}{l}\right)\cos\left(\frac{2\pi z}{l}\right)$$
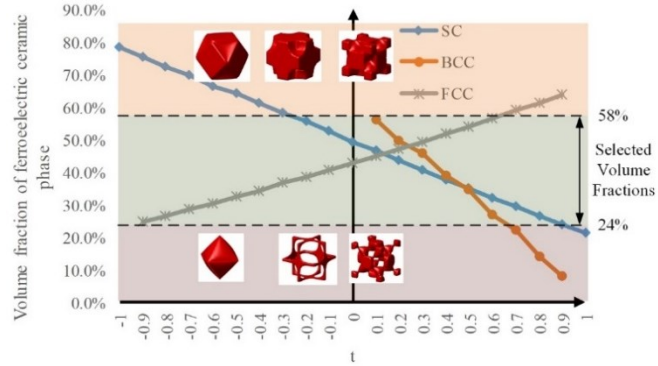$$+ \cos\left(\frac{2\pi z}{l}\right)\cos\left(\frac{2\pi x}{l}\right) + t = 0 \tag{2}$$

$$f_{fcc}(x,y,z) = 4\cos\left(\frac{2\pi x}{l}\right)\cos\left(\frac{2\pi y}{l}\right)\cos\left(\frac{2\pi z}{l}\right) + \cos\left(\frac{4\pi x}{l}\right)\cos\left(\frac{4\pi y}{l}\right)$$
$$+ \cos\left(\frac{4\pi y}{l}\right)\cos\left(\frac{4\pi z}{l}\right) + \cos\left(\frac{4\pi z}{l}\right)\cos\left(\frac{4\pi x}{l}\right) + t = 0 \tag{3}$$

where (x, y, z) is the coordinate of a point on the interface, l is the edge length of the bounding box of a unit cell, t is a constant that determines the volume fraction of the phase inside the interface with respect to the unit cell.

By changing the value of parameter t in equations (1)-(3), different interfaces representing different volume fractions of ceramics can be generated, as demonstrated in Figure 2. Given a specific volume fraction, its corresponding parameter t can be obtained from the relationships given in Figure 3, which were calculated from the solid triangular mesh of each level set structure. Note that only those interfaces with interconnected pores and no pinch-off [26] are used.

Figure 2. Phase interfaces of simple cubic, face-centered-cubic and body-centered-cubic with different volume fractions of ceramics
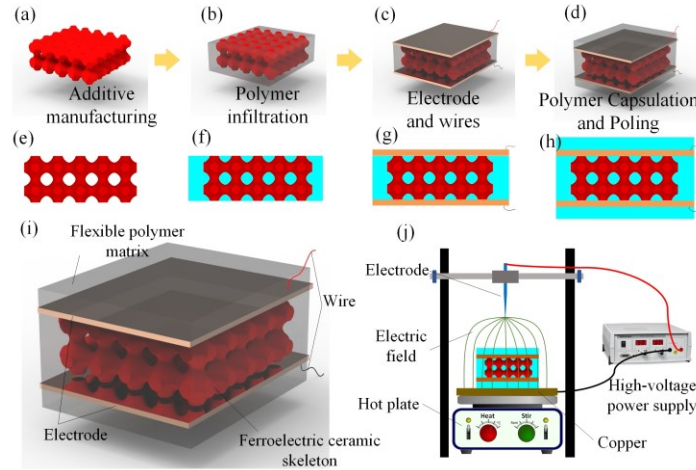

Figure 3. The relationships between volume fraction of ceramic phase and parameter t

3. Fabrication method

After a phase interface is defined for a TPC piezocomposite, the volume within the interface is designed as the ferroelectric ceramic phase and that outside the interface as the flexible polymer phase. To construct this TPC piezocomposite, the volume inside the interface is first converted into a computer-aided-design (CAD) model of the ceramic phase. The CAD model is then input into a newly developed AM process to build a ceramic lattice structure, as shown in Figure 4a and e. Afterwards, the

interconnected pores within the ceramic lattice structure are infiltrated with a flexible polymer, as shown in Figure 4b and f. The flexible polymer together with the ceramic phase comprise the TPC piezocomposite structure containing the defined phase interface. Following that, the obtained TPC piezocomposite structure undergoes post-processing, including electroding, wiring and poling, to induce piezoelectric functionalities (refer to Figure 4c, d, g and h).
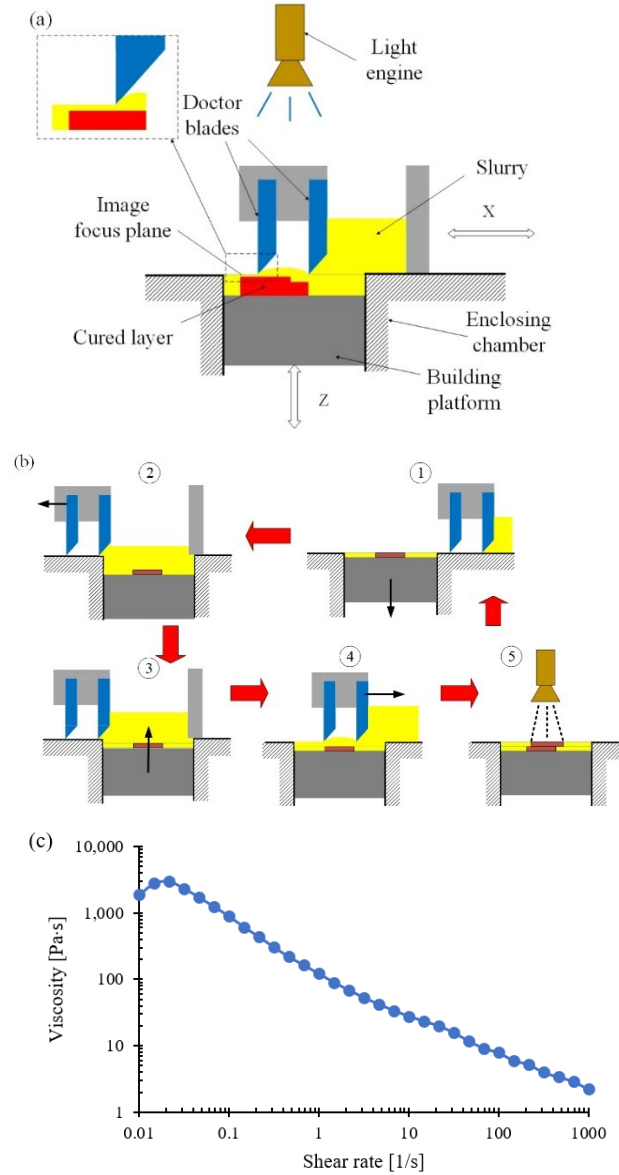

Figure 4. Schematic of sample preparation process and the corona poling apparatus

3.1 AM of piezoelectric ceramic phase

Stereolithography has been used to fabricate complex ceramic components since the 1990s [27, 28]. In this process, a mixture of ceramic powders and photocurable binder is solidified by a light source into a 3D object in a layer-by-layer manner. The 3D object, which is comprised of ceramic particles and organic binders, is then heated in furnaces to burn out the binder and densify the ceramic particles. The densified ceramic part of interest is left behind as the final product. In our prior research [29, 30], piezoelectric ceramic structures have been successfully fabricated via a tape-casting-integrated stereolithography process. However, this process has limitations in fabricating triply periodic piezoelectric lattice structures presented above. That is because these structures can easily delaminate or crack under the force generated during the process, in particularly when the porosity is high, as a result of a small bonding force between neighboring layers [29, 30] caused by the extremely low photosensitivity of the feedstock materials.

In this research, a Suspension-Enclosing Projection-Stereolithography (SEPS) process is used to fabricate the piezoelectric ceramic phase. The SEPS fabrication system is described in Figure 5a. The system consists of an enclosing chamber, a light engine, a cure platform, a double-doctor blade and a slurry container. The slurry container is filled with a piezoelectric ceramic slurry with a high yield stress. The viscosity of a 60wt% BTO slurry used in this study is given in Figure 5c. This material exhibits a

solid-like behavior when the shear stress is low. This rheological property enables the use of a free-surface coating mechanism to achieve layer recoating in the SEPS process, i.e. coating a thin slurry layer with its surface exposure to the air. This free surface layer-recoating mechanism eliminates the layer separation procedure required in traditional SLA processes [31-33] and thereby avoid potential delamination or cracking resulting from the layer separation procedure. Moreover, the SEPS process holds a promise for fabricating high-porosity structures through a static suspension-enclosing method, which can protect the structures from damage under hydrodynamic forces introduced by the process movement. More details can be found in our recent paper [34, 35].

Figure 5. (a) and (b) Schematic of the Suspension-Enclosing Projection Stereolithography process; (c) viscosity of the used BTO slurry (60 wt%)

The SEPS fabrication process is described in Figure 5b. The fabrication steps are summarized as follows: the double doctor blade is positioned at the right side of the system and its container is filled with a piezoelectric ceramic slurry (step 1). When the fabrication is initialized, the cure platform moves down for a distance d, the doctor blades move across the cure platform and fill the volume enveloped by the platform and the chamber with slurry. Then the platform moves up for a distance d-δ. Following that, the doctor blades move from left to its original position and spread the slurry into a thin layer with a thickness of δ (for BTO, δ was set to 50 μm). Finally, the light engine is activated to project an image pattern on the surface of the slurry. These procedures are repeated until a 3D object is finished.

A lattice structure fabricated by the SEPS process contains both ferroelectric ceramic particles and undesired polymeric binders. Therefore, two post-processing steps are required to remove the polymeric binder and densify the ceramic particles of interest left behind, including debinding and sintering [29, 30]. Debinding was performed in an argon atmosphere in a tube furnace (STF150, Carbolite-Gero LLC, Hope Valley, UK). The heating rate was 1°C/min. The debinding dwell time and temperature were 600°C for 180 minutes. Sintering was carried out in air under atmospheric pressure in a regular muffle furnace (HTF18, Carbolite-Gero LLC, Hope Valley, UK) with a dwell temperature of 1330°C for 240 minutes. More details about the temperature schedules for the debinding and sintering processes were discussed in our previous work. Interested readers may refer to [29, 30].

3.2 Polymer infiltration process

The obtained ferroelectric ceramic lattice structure has interconnected micro-pores that require to be infiltrated with flexible polymers to form a TPC piezocomposite. The polymer used in this study is Polydimethylsiloxane (PDMS, Sylgard-184, Dow Corning, Michigan, US). This elastomer material has a viscosity of 3500Cp [36] before curing and a Young's modulus of about 2MPa [37] after curing and is suitable for the infiltration. The infiltration was performed in a vacuum for 12 hours to allow a full saturation of pores inside the lattice by the PDMS liquid. Only the volume between top and bottom surfaces of the lattice structure was infiltrated with PDMS. Finally, the piezoelectric-ceramic lattice structure together with the infiltrated PDMS was heated at 100°C until the PDMS was fully cured. Any excess PDMS beyond the top and bottom surfaces was removed with a cutter.

3.3 Electroding and poling

The TPC piezocomposite achieved so far exhibits no piezoelectric properties until the following post-processes are conducted. Both top and bottom surfaces of the TPC piezocomposite were first coated with

silver ink or copper tapes as the electrodes. An electrical wire was soldered onto each electrode (refer to Figure 4c and g), and the TPC piezocomposite structure with electrodes and wires was capsulated with more PDMS. The final structure is given in Figure 4i.

As the last step, poling was performed to induce piezoelectricity in the TPC piezocomposite structure. In this research, all samples were poled using a corona discharge technique [13, 17, 20, 38]. The corona poling technique uses a corona needle to apply an electric field between the sample surfaces. The corona needle was put 35mm above a copper plate on a hot plate, and the applied electric field was 13kV. The temperature of the hot plate was set to 115°C and the poling period was for 10 minutes. An apparatus used for the corona poling is shown in Figure 4j.
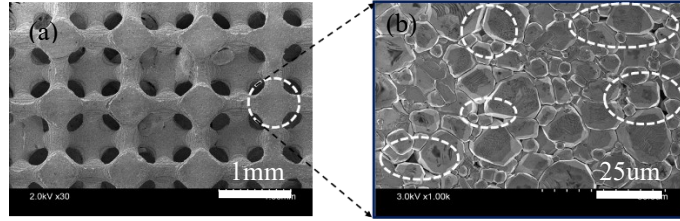
4. Property analysis

Piezoelectric properties of TPC piezocomposites are investigated in this section by both numerical and experimental approaches. Finite Element Method (FEM) is used to understand how phase interfaces and volume fractions of ceramic phase influence the overall piezoelectric properties. Triply periodic phase interfaces are also compared with traditional porous interfaces reported in the literature [20]. Furthermore, experimental analysis is performed to investigate the performance of TPC piezocomposites with different phase interfaces and volume fractions in reacting to different strains.

4.1 Numerical analysis

In this work, a two-scale model was employed to understand how phase interfaces and volume fractions of ceramic phase influence the overall piezoelectric properties of TPC piezocomposites, including a lower ceramic scale and an upper composite scale.

At the lower ceramic scale, porosity in the piezoelectric ceramic phase of a TPC piezocomposite was considered. Piezoelectric ceramics achieved by the SEPS process contain plenty of micro-pores as depicted in the Scanning Electron Microscope (SEM) images in Figure 6, which could have significant effects on mechanical and piezoelectric properties of final product as reported in the literature [15, 19, 39]. These pores are mainly located at grain boundaries (GBs) as shown in Figure 6b, which were marked by white dashed circles. According to the density measurements of the ceramic samples fabricated by the SEPS process, the porosity of the samples ranges from 5% to 10%, which is slightly higher than porosity (2~4%) of traditionally-processed ceramics [40-45]. At this scale, the widely used phase-field grain growth model [46, 47] was adopted to generate porous microstructures in the ceramic phase based on experimentally microstructural SEM images, and a fast spectral iterative perturbation method (FSIPM) was utilized to predict the piezoelectric properties of the generated porous ceramic microstructures [44].

At the upper composite scale, the effective piezoelectric properties of ceramics obtained at the lower ceramic scale were input into the composite model, where piezoelectric properties were calculated using geometrically nonlinear microstructure-sensitive finite-element simulations[18].

Figure 6. (a) A sample SEM image of an FCC specimen; (b) an image of the detailed grain structure. Pores of irregular shape can be observed as marked by white dashed circles.

4.1.1 Ceramic scale

Phase-field grain growth model was employed to regenerate the microstructures based on experimentally characterized features of pores including the locations and volume fractions of pores. Specifically, in the phase-field model, a set of order parameters $\{\eta_g\}_{g=1,...G}$ was used to describe the G grains, which vary continuously from 0 to 1 at GBs and equal 1 within grains.

Since pores are mainly located at GBs [24, 30, 31] and the values of order parameters vary continuously from 0 to 1 at GBs, targeted volume fractions of pores could be readily acquired by setting the square of order parameters smaller than certain value, for instance $\{\eta_g^2\}_{g=1,...G} \leq 0.557$, corresponding which the phase would be defined as pore phase. In this work, as a representative, a roughly average value 8% volume fraction of porosity was considered. Following that, the FSIPM was adopted to calculate the piezoelectric properties of the porous ceramics, which is an efficient and direct numerical algorithm for solving equilibrium equations in a periodic system, especially for the system in this work with inhomogeneous properties [48-50]

4.1.2. Composite scale

A representative elementary volume (RVE) is used in the FEM to predict the piezoelectric properties of the polymer-ceramic composites under different stimuli. BTO was selected as the materials in the calculation. The material properties are shown in Table 1. The piezoelectric constitutive equations that couple the mechanical and electric fields are:

$$\{\mathbf{D}\} = [\mathbf{e}]\{\mathbf{\varepsilon}\} + [\mathbf{\chi}]\{\mathbf{E}\} \qquad (4)$$

$$\{\sigma\} = [C]\{\epsilon\} - [e]\{E\}$$

where $\{D\}$ is the electric displacement vector, $\{\sigma\}$ is the stress tensor, $\{\varepsilon\}$ is the strain tensor, $\{E\}$ is the electric field, $[C]$ is the elastic stiffness matrix, $[e]$ is the piezoelectric matrix and $[\chi]$ is the dielectric permittivity matrix at a constant mechanical stress. Specifically, the mechanical strain involves both geometrically linear and nonlinear parts by taking into account the large deformation originated from the "soft" nature of polymer subjected to a certain large mechanical loading, as $\varepsilon = \varepsilon_L + \varepsilon_{NL}$, where $\varepsilon_{L,ij} = \frac{1}{2}\left(u_{i,j} + u_{j,i}\right)$ and $\varepsilon_{NL,ij} = \frac{1}{2}\left(u_{k,i}u_{k,j}\right)$. Here, $\{u\}$ is the displacement vector solved from the stress equilibrium equation using FEM. All the governing equations together with the numerical schemes are implemented through a commercial finite-element software package, COMSOL 5.2. The periodic boundary conditions are used for RVE. To establish grid independence, the system mesh was set with a smallest element size of 0.05mm based on solution convergence trials. A tensile stress of 0.2 GPa is applied at the surfaces along the poling direction, i.e., z-direction. Note that indices 1, 2, and 3 represent the x-, y-, and z-axes. No external electric field is applied to the RVE.

Table 1. Material piezoelectric coefficient ($10^{-12}mV^{-1}$)[51, 52]

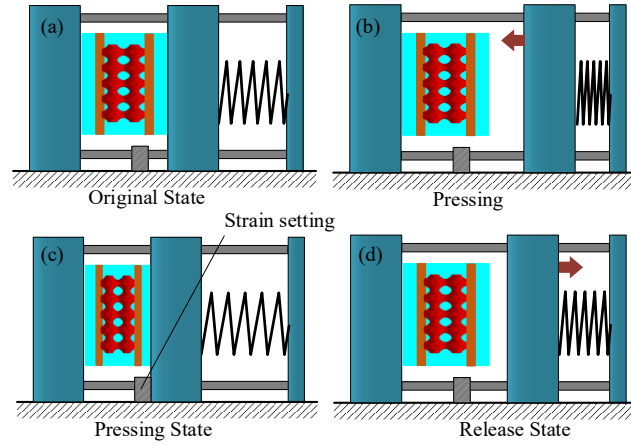| Coefficient	PDMS	BTO
d_{31}	-2.4	-23.2
d_{32}	-2.4	-23.2
d_{33}	7.45	70.7

4.2 Experimental analysis

Piezoelectric properties of TPC piezocomposites fabricated by the presented method were experimentally analyzed through both a voltage-response test and piezoelectric constant measurement:

For voltage-response tests, TPC piezocomposites with different phase interfaces and volume fractions were fabricated using the SEPS process. According to Figure 3, a volume fraction between 24% and 58% enables optimal interface architectures with fully interconnected pores and no pinch-off. Meanwhile, a ceramic lattice with a volume fraction higher than 40% possesses sufficient mechanical strength. In this study, three volume fractions of ceramic were selected for each type of phase interface, including 44%, 50% and 56%. Parameter t corresponding to each volume fraction and phase interface is given in Table 2. Nine samples were fabricated for the experimental analysis in total. The piezoelectric responses of each

sample were measured under pressing mode through a homemade linear pressing station, as described in Figure 7a-d. A probe in the linear pressing station was controlled to press the sample for a given distance at a speed of 5mm/s. The ratio between the given pressing distance and the original thickness of the sample is defined as strain. Three strain values were applied in the experiments, including 3.33%, 6.67% and 10%. After that, the sample was released, and its voltage responses were recorded via an oscilloscope. This pressing-releasing movement was repeated until stable voltage responses were obtained.

For piezoelectric constant measurement, three samples of each type of phase interface with 50%±5% volume fraction of ceramics were fabricated. Piezoelectric charge constant d33 of each sample was measured using a d33 meter (APC International, Ltd., Mill Hall, PA, USA) at a force frequency of 110Hz. Permittivity ε was measured using an LCR meter at 1kHz. Piezoelectric voltage constant g33 was calculated via the equation g33=d33/$\varepsilon_r\varepsilon_0$[53].

Figure. 7. Testing procedures for voltage responses of TPC piezocomposites.

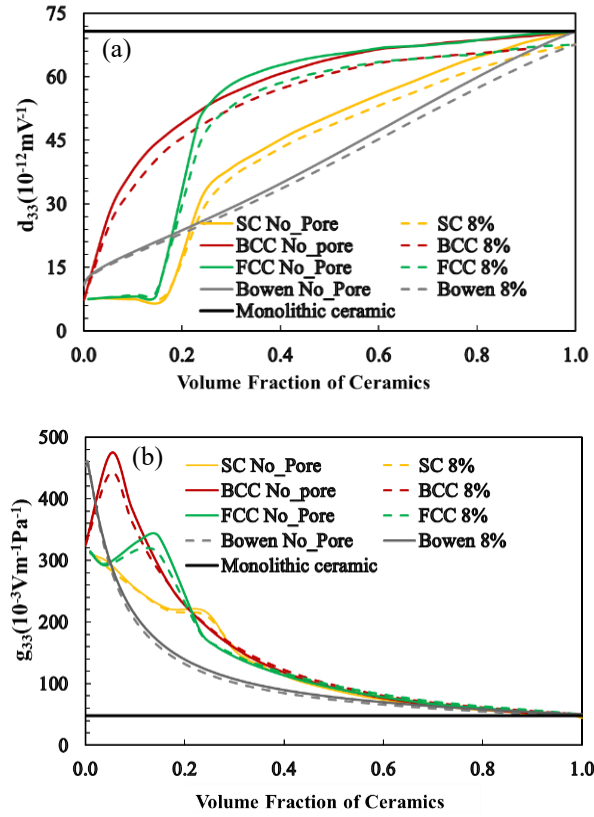**Table 2**. Parameter t for selected phase interfaces and volume fractions

VF / Type	44%	50%	56%
SC	-1	-0.5	0
BCC	-0.7	-0.5	-0.2
FCC	0.9	0.4	-0.3

5. Results

The results of numerical and experimental analysis are discussed in this section.

5.1 Numerical results

First, in order to validate our model, the piezoelectric charge constant d_{33} of the TPC piezocomposites were compared with that of the traditional 3-3 piezocomposites with porous phase interface presented by Bowen [18] . As can be noticed in Figure 8, the d_{33} of all the structures increases with higher volume fraction of ceramics, since the ceramic is the main source of piezoelectricity [15, 17, 21, 54]. However, piezoelectric voltage constant, $g_{33}=d_{33}/\varepsilon_{33}$, of all the structures decreases with increasing volume fraction of ceramics, which may be attributed to modest increase of d_{33} but rapid increase of permittivity ε_{33} as depicted in Figure 9.
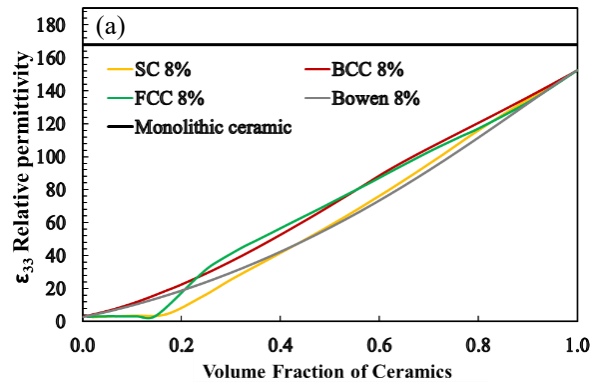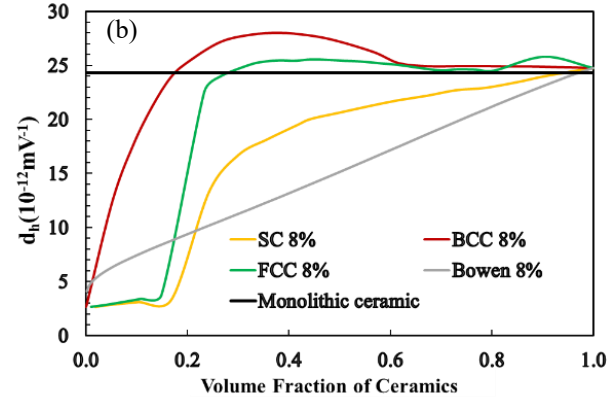

Figure. 8. The d_{33} (a) and g_{33} (b) comparison between different TPC piezocomposites and Bowen's structure with the increasing volume fractions of ceramics.

Porosity effect is not so significant due to low-level porosity existing in ceramics, as shown in Figure 8 and 9. For example, the d_{33} of SC without porosity at volume fraction of 50% ceramics is 50.768 $10^{-12}mV^{-1}$ while with 8% volume fraction of porosity, d_{33} is 48.3774 $10^{-12}mV^{-1}$. Similarly, the g_{33} of TPC composites with porosity are just slightly decreased compared to those without porosity, which may be explained by simultaneous decrease of d_{33} and ε_{33} due to the existence of pores, whose d_{33} and ε_{33} is 0 and 1, respectively.
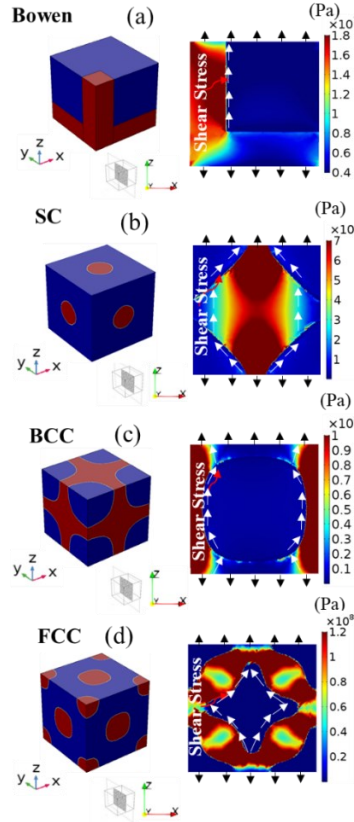
13

Moreover, all the piezoelectric properties of the TPC piezocomposites with SC and FCC interfaces increase dramatically at the volume fraction of around 20%. This is because those structures become 3D interconnected at this volume fraction, as inherently determined by those periodic equations adopted to define TPC structures. In addition, within the range of 25%~60% volume fraction, hydrostatic piezoelectric strain constant d_h of all TPC piezocomposites tends to become stable at the volume fraction of 60%, as shown in Figure 9b. This suggests that the volume fraction of ceramics with the optimal overall performance is located in the range of 25%~60%, which corresponds to configurations featuring the best interconnectivity of ceramic and polymer phases in TPC piezocomposites, as shown in Figure 3.

Furthermore, all the TPC piezocomposites outperform the traditional 3-3 piezocomposites with porous phase interface presented by Bowen [18], in particular when the volume fraction of ceramic phase is greater than 20%. This is attributed to a larger stress transfer efficiency of triply periodic minimal interfaces than the traditional porous interface, as shown in Figure 10. Of particular interest is the result that the three triply periodic minimal interfaces achieve distinct piezoelectric properties in the TPC piezocomposites, even with the same volume fraction of ceramics. To be specific, with the same volume fraction of ceramics, particularly in the range of 25%-60%, BCC and FCC are superior to SC. The difference in piezoelectric performance of the three TPC piezocomposites may be explained by their stress transfer efficiency discrepancy as shown in Figure 10.

Figure. 9. Relative permittivity ε_{33} and hydrostatic piezoelectric strain constants trends of TPC piezocomposites and traditional 3-3 piezocomposite.

Figure. 10. Stress transfer efficiency comparison of TPC piezocomposite and traditional 3-3 piezocomposite.

5.2 Experimental results

The fabricated TPC piezocomposites with the configurations in Table 2 are shown in Figure 11 and Figure 12. Each of the TPC piezocomposite structures has 5 periodic units along its X and Y direction

and 2 periodic units along the Z direction, as shown in the insets of Figure 11a-c. One periodic unit has a dimension of 2×2×2mm and has a phase interface defined by the equations (1)-(3). The overall dimension of each sample is 10×10×4mm. Three fabricated green parts with SC, BCC and FCC phase interfaces are shown in Figure 11a-c. Their volume fractions of ceramics are 44%. Debinding and sintering these green parts yield the piezoelectric ceramic lattices shown in Figure 11d-l. Microscope images of these ceramic lattices in XY plane and Z direction are shown in Figure 11g-i and Figure 11j-l respectively. The linear shrinkage before and after the debinding and sintering processes for all the lattices was measured as 31% ± 0.5%. The final TPC piezocomposites after infiltrating PDMS are demonstrated in Figure 12. The interfacial bonding between the infiltrated PDMS and the ceramic phase was mainly due to the surface roughness of the BTO lattices resulting from staircase effect. This bonding strength was expected to be low but can be further enhanced by pretreating the surface of the ceramic lattices with coupling agents, whose effect on the piezoelectric properties of TPC piezocomposites will be explored in our future work.

Voltage responses obtained through the linear pressing station are given in Figure 13. The voltage responses of the 44% TPC piezocomposites under different strains are shown in Figure 13a-c. Each of these TPC piezocomposite components exhibits a mechanical flexibility under a strain up to 10%. When a higher strain is applied, the components generate a higher voltage output.
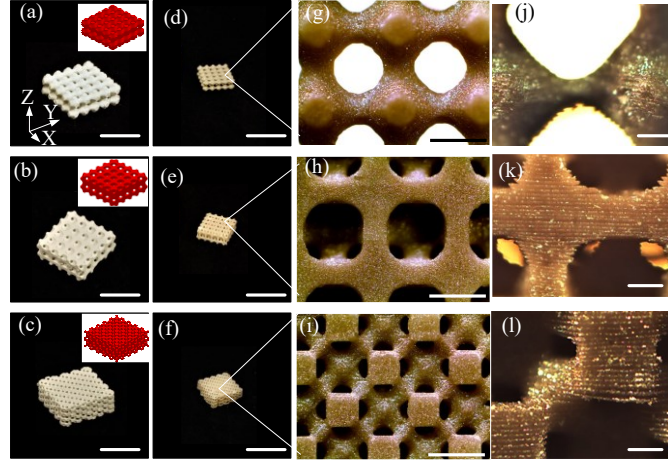
Figure 13d-f show how the volume fractions of ceramics influence the voltage responses in each type of TPC piezocomposites. The same strain of 10% was applied to each sample. The experimental results indicate that a lower volume ratio of ceramics appears to yield a higher voltage response, which agrees well with the numerical simulation result of piezoelectric voltage constant g_{33} in Figure 8b. Potential reasons are that a lower volume fraction of ceramics introduces a higher ratio of flexible polymer, leading to a lower relative permittivity and a lower elastic stiffness. A further study of the volume fraction will be performed in our future work.

TPC piezocomposites with different phase interfaces are compared under different strains, as depicted in Figure 13g-i. The volume fraction of ceramics was set as 44%. It can be seen that BCC and FCC interfaces result in a greater voltage response than SC. In comparison to the voltage responses obtained under the strain 3.33% and 6.67%, the difference in the responses of SC, BCC and FCC achieved under the strain 10% is smaller. This smaller difference may be caused by the reduced stress transfer between the PDMS and the active ceramic phase in all the three architectures as a result of interfacial slippage under the strain 10%.
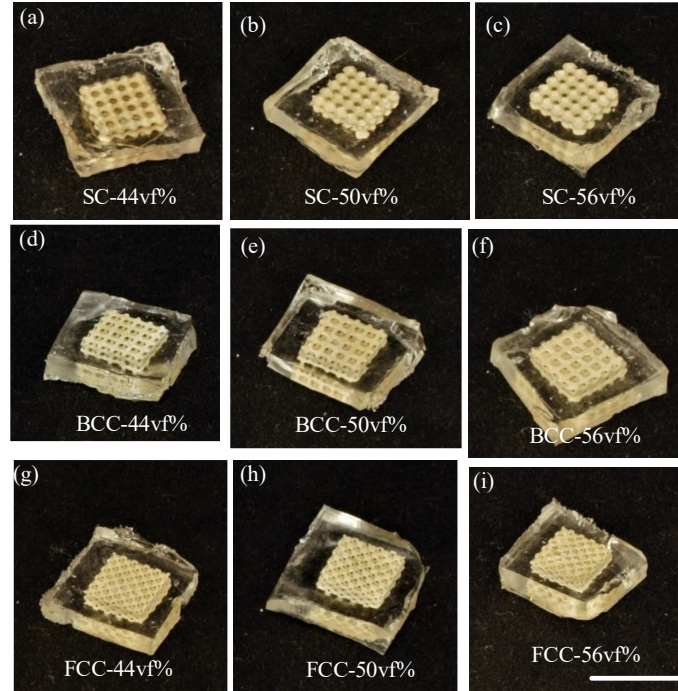
The finding of higher-performance of BCC and FCC than SC agrees well with the property characterization results as depicted by Figure 14. The variation in the piezoelectric properties of the three samples corresponding to the same phase interface is caused by the difference in the achieved volume fraction of ceramics with a tolerance of ±5%. The difference between the result of experimental and
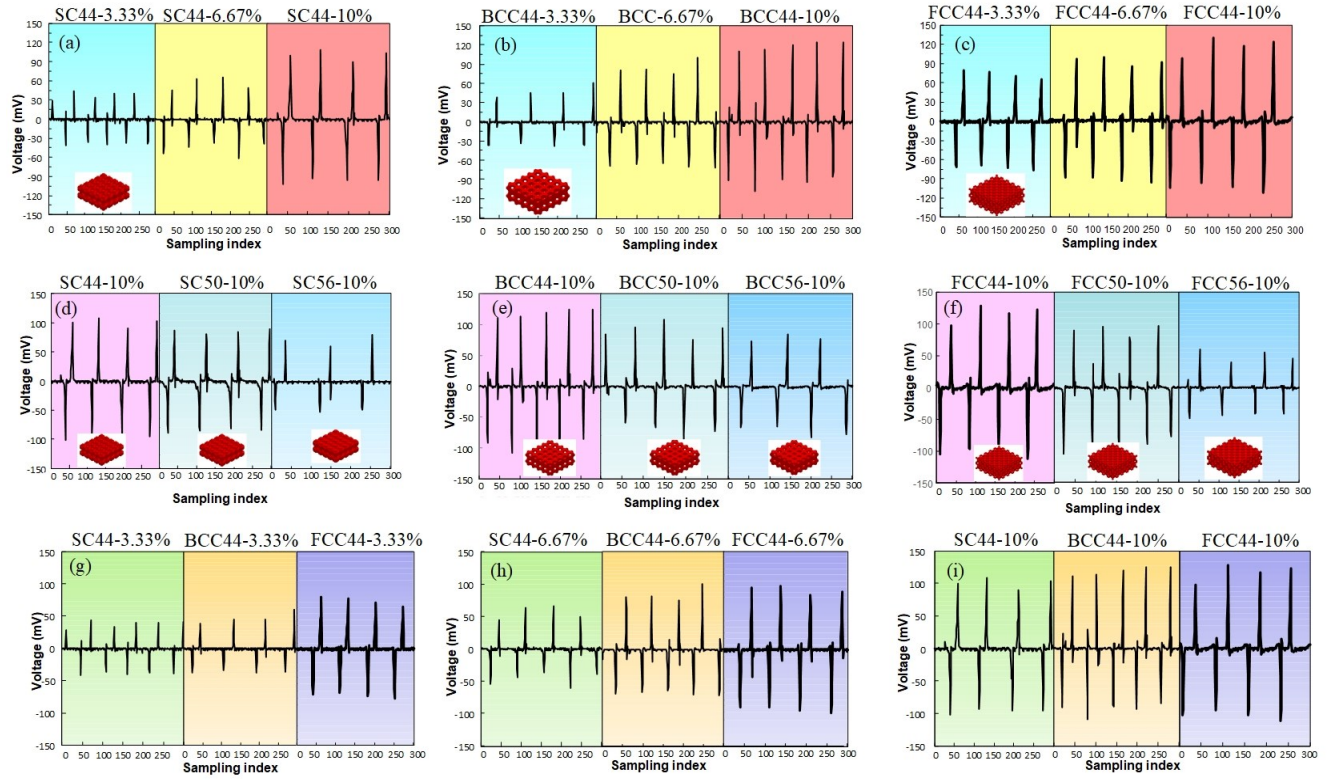
numerical analysis could be attributed to other effects not considered in the current model, such as interface effect between polymer and ceramic[17, 55], and/or grain orientation effect [44], which will be the focus of our future work.
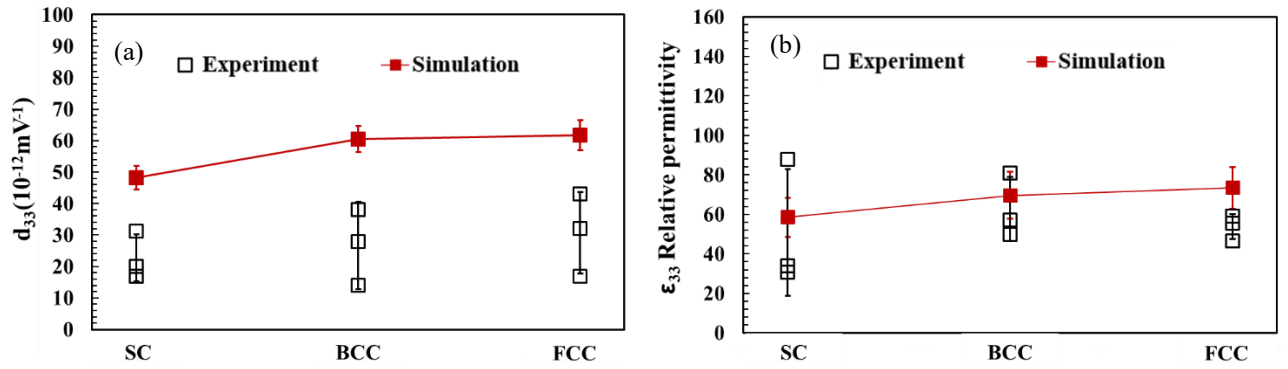

Figure. 11. Fabrication results: (a-c) green parts; (d-l) piezoelectric ceramic lattices; Scale bar: (a-f)10 mm; (g-i)1 mm; (j-l)500 μm;
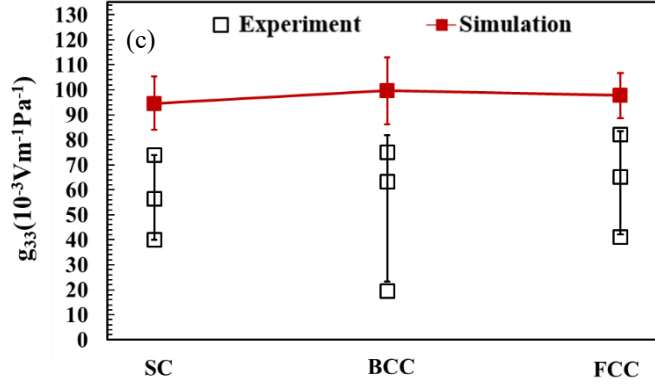

Figure. 12. Fabrication results of TPC piezocomposites. Scale bar: 10 mm.

Figure 13. Voltage responses of TPC piezocomposites. (a-c) effects of strains. (d-f) effects of volume fractions of ceramics. (g-i) effects of phase interfaces.

Figure. 14. Result comparison between experiment measurement and numerical analysis for TPC piezocomposites with 2% volume fraction of porosity.

6. Conclusion

In this research, a highly tailorable 3-3 architecture called triply periodic bi-continuous piezocomposites or TPC piezocomposites are presented to achieve two seemingly conflicting properties of mechanical flexibility and piezoelectricity in piezoelectric materials. This new architecture is comprised of two continuously interconnected phases, i.e. an active piezoelectric ceramic phase and a passive flexible polymeric phase, which are separated by a predefined phase interface. Triply periodic minimal surfaces are used in the design of phase interfaces due to their large elastic constants. An additive manufacturing process called Suspension-Enclosing Projection-Stereolithography is used to fabricate this piezocomposite.

Compared with state-of-the-art piezoelectric materials, the presented TPC piezocomposites exhibit mechanical flexibility under loads and feature a superb hydrostatic piezoelectricity which shows their great potential in underwater acoustic devices. Their piezoelectric properties were analyzed by both numerical and experimental methods.

In the future, more piezoelectric properties of the presented TPC piezocomposites will be experimentally studied. A design framework will be studied to optimize the geometry of the phase interface, in order to achieve an optimal combination of piezoelectricity and flexibility.

Reference

[1]   Kumar, S., and Singh, R. N., 1996, "Crack propagation in piezoelectric materials under combined mechanical and electrical loadings," Acta materialia, 44(1), pp. 173-200.
[2]   Gullapalli, H., Vemuru, V. S., Kumar, A., Botello‑Mendez, A., Vajtai, R., Terrones, M., Nagarajaiah, S., and Ajayan, P. M., 2010, "Flexible piezoelectric ZnO–paper nanocomposite strain sensor," small, 6(15), pp. 1641-1646.
[3]   Skinner, D., Newnham, R., and Cross, L., 1978, "Flexible composite transducers," Materials Research Bulletin, 13(6), pp. 599-607.
[4]   Kim, H. S., Kim, J.-H., and Kim, J., 2011, "A review of piezoelectric energy harvesting based on vibration," International journal of precision engineering and manufacturing, 12(6), pp. 1129-1141.
[5]   Bowen, C., Kim, H., Weaver, P., and Dunn, S., 2014, "Piezoelectric and ferroelectric materials and structures for energy harvesting applications," Energy & Environmental Science, 7(1), pp. 25-44.
[6]   O'Donnell, J., Kim, M., and Yoon, H.-S., 2017, "A review on electromechanical devices fabricated by additive manufacturing," Journal of Manufacturing Science and Engineering, 139(1), p. 010801.
[7]   Kao, Y.-T., Zhang, Y., Wang, J., and Tai, B. L., 2017, "Loading–Unloading Cycles of Three-Dimensional-Printed Built Bimaterial Structures With Ceramic and Elastomer," Journal of Manufacturing Science and Engineering, 139(4), p. 041006.
[8]   Newnham, R., Skinner, D., and Cross, L., 1978, "Connectivity and piezoelectric-pyroelectric composites," Materials Research Bulletin, 13(5), pp. 525-536.
[9]   Tressler, J., Alkoy, S., Dogan, A., and Newnham, R., 1999, "Functional composites for sensors, actuators and transducers," Composites Part A: Applied Science and Manufacturing, 30(4), pp. 477-482.
[10]   Bowen, C., and Topolov, V. Y., 2003, "Piezoelectric sensitivity of PbTiO 3-based ceramic/polymer composites with 0–3 and 3–3 connectivity," Acta materialia, 51(17), pp. 4965-4976.
[11]   Han, K., Safari, A., and Riman, R. E., 1991, "Colloidal Processing for Improved Piezoelectric Properties of Flexible 0–3 Ceramic–Polymer Composites," Journal of the American Ceramic Society, 74(7), pp. 1699-1702.
[12]   Van Loock, F., Deutz, D., van der Zwaag, S., and Groen, W., 2016, "Exploring the piezoelectric performance of PZT particulate-epoxy composites loaded in shear," Smart Materials and Structures, 25(8), p. 085039.
[13]   Taunaumang, H., Guy, I., and Chan, H. L., 1994, "Electromechanical properties of 1‑3 piezoelectric ceramic/piezoelectric polymer composites," Journal of applied physics, 76(1), pp. 484-489.
[14]   Lous, G. M., Cornejo, I. A., McNulty, T. F., Safari, A., and Danforth, S. C., 2000, "Fabrication of piezoelectric ceramic/polymer composite transducers using fused deposition of ceramics," Journal of the American Ceramic Society, 83(1), pp. 124-128.
[15]   Banno, H., 1993, "Effects of porosity on dielectric, elastic and electromechanical properties of Pb (Zr, Ti) O3 ceramics with open pores: a theoretical approach," Japanese journal of applied physics, 32(9S), p. 4214.
[16]   Bowen, C., Perry, A., Kara, H., and Mahon, S., 2001, "Analytical modelling of 3-3 piezoelectric composites," Journal of the European Ceramic Society, 21(10), pp. 1463-1467.

[17]   Kara, H., Ramesh, R., Stevens, R., and Bowen, C. R., 2003, "Porous PZT ceramics for receiving transducers," IEEE transactions on ultrasonics, ferroelectrics, and frequency control, 50(3), pp. 289-296.
[18]   Ji, Y. Z., Wang, Z., Wang, B., Chen, Y., Zhang, T., Chen, L. Q., Song, X., and Chen, L., 2017, "Effect of Meso‑Scale Geometry on Piezoelectric Performances of Additively Manufactured Flexible Polymer–Pb (ZrxTi1– x) O3 Composites," Advanced Engineering Materials.
[19]   Nguyen, B., Challagulla, K., Venkatesh, T., Hadjiloizi, D., and Georgiades, A., 2016, "Effects of porosity distribution and porosity volume fraction on the electromechanical properties of 3-3 piezoelectric foams," Smart Materials and Structures, 25(12), p. 125028.
[20]   Roscow, J., Lewis, R., Taylor, J., and Bowen, C., 2017, "Modelling and fabrication of porous sandwich layer barium titanate with improved piezoelectric energy harvesting figures of merit," Acta Materialia, 128, pp. 207-217.
[21]   Roscow, J., Zhang, Y., Taylor, J., and Bowen, C., 2015, "Porous ferroelectrics for energy harvesting applications," Eur. Phys. J.-Spec. Top, 224, p. 2949.
[22]   Maldovan, M., Ullal, C. K., Jang, J. H., and Thomas, E. L., 2007, "Sub‑Micrometer Scale Periodic Porous Cellular Structures: Microframes Prepared by Holographic Interference Lithography," Advanced Materials, 19(22), pp. 3809-3813.
[23]   Wang, L., Lau, J., Thomas, E. L., and Boyce, M. C., 2011, "Co‑continuous composite materials for stiffness, strength, and energy dissipation," Advanced Materials, 23(13), pp. 1524-1529.
[24]   Chen, Y., and Wang, L., 2014, "Periodic co-continuous acoustic metamaterials with overlapping locally resonant and Bragg band gaps," Applied Physics Letters, 105(19), p. 191907.
[25]   Góźdź, W. T., and Hołyst, R., 1996, "Triply periodic surfaces and multiply continuous structures from the Landau model of microemulsions," Physical Review E, 54(5), p. 5012.
[26]   Lambert, C. A., Radzilowski, L. H., and Thomas, E. L., 1996, "Triply periodic level surfaces as models for cubic tricontinuous block copolymer morphologies," Philosophical Transactions of the Royal Society of London A: Mathematical, Physical and Engineering Sciences, 354(1715), pp. 2009-2023.
[27]   Halloran, J. W., 2016, "Ceramic stereolithography: additive manufacturing for ceramics by photopolymerization," Annual Review of Materials Research, 46, pp. 19-40.
[28]   Song, X., Zhang, Z., Chen, Z., and Chen, Y., 2017, "Porous structure fabrication using a stereolithography-based sugar foaming method," Journal of Manufacturing Science and Engineering, 139(3), p. 031015.
[29]   Song, X., Chen, Z., Lei, L., Shung, K., Zhou, Q., and Chen, Y., 2017, "Piezoelectric component fabrication using projection-based stereolithography of barium titanate ceramic suspensions," Rapid Prototyping Journal, 23(1).
[30]   Chen, Z., Song, X., Lei, L., Chen, X., Fei, C., Chiu, C. T., Qian, X., Ma, T., Yang, Y., and Shung, K., 2016, "3D printing of piezoelectric element for energy focusing and ultrasonic sensing," Nano Energy, 27, pp. 78-86.
[31]   Ye, H., Venketeswaran, A., Das, S., and Zhou, C., 2017, "Investigation of separation force for constrained-surface stereolithography process from mechanics perspective," Rapid Prototyping Journal, 23(4), pp. 696-710.
[32]   Pan, Y., He, H., Xu, J., and Feinerman, A., 2017, "Study of separation force in constrained surface projection stereolithography," Rapid Prototyping Journal, 23(2), pp. 353-361.
[33]   He, H., Xu, J., Yu, X., and Pan, Y., 2018, "Effect of Constrained Surface Texturing on Separation Force in Projection Stereolithography," Journal of Manufacturing Science and Engineering, 140(9), p. 091007.
[34]   He, L., and Song, X., 2017, "Supportability of a High-Yield-Stress Slurry in a New Stereolithography-Based Ceramic Fabrication Process," JOM.

[35]   He, L., Fei, F., Wang, W., and Song, X., 2019, "Support-Free Ceramic Stereolithography of Complex Overhanging Structures Based on an Elasto-viscoplastic Suspension Feedstock," ACS applied materials & interfaces.

[36]   Corning, D., "Sylgard 184 Silicone Elastomer," http://www.dowcorning.com/DataFiles/090276fe80190b08.pdf.

[37]   Johnston, I., McCluskey, D., Tan, C., and Tracey, M., 2014, "Mechanical characterization of bulk Sylgard 184 for microfluidics and microengineering," Journal of Micromechanics and Microengineering, 24(3), p. 035017.

[38]   Waller, D., Iqbal, T., and Safari, A., 1989, "Poling of lead zirconate titanate ceramics and flexible piezoelectric composites by the corona discharge technique," Journal of the American Ceramic Society, 72(2), pp. 322-324.

[39]   Dunn, M. L., 1995, "Effects of grain shape anisotropy, porosity, and microcracks on the elastic and dielectric constants of polycrystalline piezoelectric ceramics," Journal of applied physics, 78(3), pp. 1533-1541.

[40]   Liu, J., Shen, Z., Yao, W., Zhao, Y., and Mukherjee, A. K., 2010, "Visible and infrared transparency in lead-free bulk BaTiO3 and SrTiO3 nanoceramics," Nanotechnology, 21(7), p. 075706.

[41]   Devan, R. S., Ma, Y.-R., and Chougule, B., 2009, "Effective dielectric and magnetic properties of (Ni–Co–Cu) ferrite/BTO composites," Materials Chemistry and Physics, 115(1), pp. 263-268.

[42]   Polotai, A., Breece, K., Dickey, E., Randall, C., and Ragulya, A., 2005, "A novel approach to sintering nanocrystalline barium titanate ceramics," Journal of the American Ceramic Society, 88(11), pp. 3008-3012.

[43]   Burke, J., 1957, "Role of Grain Boundaries in Sintering," Journal of the American Ceramic Society, 40(3), pp. 80-85.

[44]   Ming, C., Yang, T., Luan, K., Chen, L., Wang, L., Zeng, J., Li, Y., Zhang, W., and Chen, L.-Q., 2018, "Microstructural effects on effective piezoelectric responses of textured PMN-PT ceramics," Acta Materialia, 145, pp. 62-70.

[45]   Chaim, R., Levin, M., Shlayer, A., and Estournès, C., 2008, "Sintering and densification of nanocrystalline ceramic oxide powders: a review," Advances in Applied Ceramics, 107(3), pp. 159-169.

[46]   Krill Iii, C., and Chen, L.-Q., 2002, "Computer simulation of 3-D grain growth using a phase-field model," Acta materialia, 50(12), pp. 3059-3075.

[47]   Chen, L. Q., 2008, "Phase‐field method of phase transitions/domain structures in ferroelectric thin films: a review," Journal of the American Ceramic Society, 91(6), pp. 1835-1844.

[48]   Hu, S., and Chen, L., 2001, "A phase-field model for evolving microstructures with strong elastic inhomogeneity," Acta materialia, 49(11), pp. 1879-1890.

[49]   Yu, P., Hu, S., Chen, L., and Du, Q., 2005, "An iterative-perturbation scheme for treating inhomogeneous elasticity in phase-field models," Journal of Computational Physics, 208(1), pp. 34-50.

[50]   Zhu, J., Chen, L.-Q., Shen, J., and Tikare, V., 1999, "Coarsening kinetics from a variable-mobility Cahn-Hilliard equation: Application of a semi-implicit Fourier spectral method," Physical Review E, 60(4), p. 3564.

[51]   Meng, X., Wen, X., and Qin, G., 2010, "DFT study on elastic and piezoelectric properties of tetragonal BaTiO3," Computational Materials Science, 49(4), pp. S372-S377.

[52]   Sharma, S. K., Gaur, H., Kulkarni, M., Patil, G., Bhattacharya, B., and Sharma, A., 2013, "PZT–PDMS composite for active damping of vibrations," Composites Science and Technology, 77, pp. 42-51.

[53]   James, N. K., Deutz, D. B., Bose, R. K., van der Zwaag, S., and Groen, P., 2016, "High Piezoelectric Voltage Coefficient in Structured Lead‐Free (K, Na, Li) NbO3 Particulate—Epoxy Composites," Journal of the American Ceramic Society, 99(12), pp. 3957-3963.

[54]   Rittenmyer, K., Shrout, T., Schulze, W., and Newnham, R., 1982, "Piezoelectric 3–3 composites," Ferroelectrics, 41(1), pp. 189-195.

[55]   Lewis, T., 2004, "Interfaces are the dominant feature of dielectrics at the nanometric level," IEEE transactions on dielectrics and electrical insulation, 11(5), pp. 739-753.

Figure Caption List

Figure 1. Constructions and properties of piezoelectric composites. (1) Main connectivity patterns of piezoelectric composites; (2) comparisons of piezoelectric materials in hydrostatic piezoelectric properties and mechanical flexibility.

Figure 2. Phase interfaces of simple cubic, face-centered-cubic and body-centered-cubic with different volume fractions of ceramics

Figure 3. The relationships between volume fraction of ceramic phase and parameter t

Figure 4. Schematic of sample preparation process and the corona poling apparatus

Figure 5. (a) and (b) Schematic of the Suspension-Enclosing Projection Stereolithography process; (c) viscosity of the used BTO slurry (60 wt%)

Figure 6. (a) A sample SEM image of an FCC specimen; (b) an image of the detailed grain structure. Pores of irregular shape can be observed as marked by white dashed circles.

Figure. 7. Testing procedures for voltage responses of TPC piezocomposites.

Figure. 8. The d_{33} (a) and g_{33} (b) comparison between different TPC piezocomposites and Bowen's structure with the increasing volume fractions of ceramics.

Figure. 9. Relative permittivity ε_{33} and hydrostatic piezoelectric strain constants trends of TPC piezocomposites and traditional 3-3 piezocomposite.

Figure. 10. Stress transfer efficiency comparison of TPC piezocomposite and traditional 3-3 piezocomposite.

Figure. 11. Fabrication results: (a-c) green parts; (d-l) piezoelectric ceramic lattices; Scale bar: (a-f)10 mm; (g-i)1 mm; (j-l)500 μm;

Figure. 12. Fabrication results of TPC piezocomposites. Scale bar: 10 mm.

Figure 13. Voltage responses of TPC piezocomposites. (a-c) effects of strains. (d-f) effects of volume fractions of ceramics. (g-i) effects of phase interfaces.

Figure. 14. Result comparison between experiment measurement and numerical analysis for TPC piezocomposites with 2% volume fraction of porosity.

Table Caption List

Table 1. Material piezoelectric coefficient ($10^{-12}mV^{-1}$)

Table 2. Parameter t for selected phase interfaces and volume fractions